Pestic. Sci. 1996, **47**, 145–158

Design of Inhibitors of Photosystem II using a Model of the D1 Protein

Ursula Egner,[a]* Klaus Peter Gerbling,[b] Georg-Alexander Hoyer,[a] Gabriele Krüger[a] & Peter Wegner[b]

[a] Research Laboratories of Schering AG, D-13342 Berlin, Germany
[b] Hoechst-Schering AgrEvo GmbH, D-13476 Berlin, Germany

(Received 19 July 1995; accepted 5 December 1995)

Abstract: Several inhibitors belonging to structurally different chemical classes were used to analyze the predictive power of an initial model of the herbicide binding niche of the D1 protein belonging to photosystem II (PS II) from plants. In the case of small PS II inhibitors, the estimation of relative activities was hampered by uncertainty about the binding modes. To overcome this problem, a bulky substituent was introduced into the inhibitors to act as a hook, resulting in an unambiguous orientation in the model. The comparison of the modelling results and the experimentally determined IC_{50} values of different triazines suggested that the previously assumed volume of the binding niche had to be reduced by 20%. After refinement of the model, it was possible to estimate qualitatively, the relative in-vitro activity for inhibitors belonging to different families, as long as an unambiguous binding mode could be deduced either from steric demands or from IC_{50} values of mutant D1 proteins. The usefulness of the refined model is demonstrated by the successful *de-novo* design of a potent class of herbicides, the triazolopyrimidines.

Key words: energy minimization, modelling, herbicide design, D1 protein.

1 INTRODUCTION

Life on earth depends on the chemical synthesis, storage and delivery of energy-rich organic compounds in plants or green algae. One of the main steps in this process is accomplished by photosystem II (PS II), which catalyses the transfer of electrons from water to plastoquinone. The specific inhibition of PS II in weeds can be accomplished by displacing the natural ligand by commercially important herbicides.[1–3] The major target for this inhibition is the D1 protein, a polypeptide with a molecular weight of 32 kD, which, because of its importance, has been the subject of various basic and applied studies by many research groups. A better knowledge of the D1 protein should facilitate the design of more selective inhibitors of this protein with low use-rates, thereby increasing the agricultural benefits and at the same time minimizing ecological damage.

Until recently, new active compounds were discovered either by random structures or imitative chemistry, i.e. variation of natural ligands or existing lead structures.[4] If structural information about the binding site is available, a rational approach is often able to support the search for active compounds. In the case of the D1 protein, no X-ray or NMR structure is known, but the crystal structures of the homologous photosynthetic reaction centres of *Rhodopseudomonas viridis* (*Rps viridis*) and *Rhodobacter sphaeroides* have been determined in 1986 and 1987.[5–8] Despite the low sequence homology, several laboratories have developed models of the herbicide binding niche of the D1 protein, based on these crystal structures.[9–14] There are several reasons why it is difficult to construct an exact model of the active site of the D1 protein: (1) The overall homology between the D1 protein and the corresponding L-subunits of the bacterial reaction centres is low. With a sequence identity at the active sites of only 20%, structural changes are to be expected. (2) Bulky amino acid residues at the active site of the bacterial reaction centre are replaced by smaller ones in the D1 protein, giving rise to a larger binding site. (3) To achieve an optimal sequence alignment, two insertions

* To whom correspondence should be addressed.

Pestic. Sci. 0031-613X/96/$09.00

of three and 14 amino acid residues, respectively, have to be accommodated in the active site of the D1 protein with respect to the bacterial proteins (Fig. 1).

These inherent difficulties with an initial three-dimensional model meant that validation and refinement of the model would be necessary and IC_{50} values determined from mutant D1 proteins or from inhibitors with varying substituents can obviously aid in this process. To test our previously published model of the active site of the D1 protein, we chose new heterobicyclic compounds which differ structurally from well-known PS II inhibitors.[9] The choice of new substituents, the chemical synthesis of the inhibitors and the comparison of the estimated and measured binding constants have—in an iterative process—improved our model. The close collaboration between theoretical chemists, bench chemists and biochemists has resulted in the successful design and synthesis of a new class of herbicides, the triazolopyrimidines.

In the following sections, we detail the refinement of our model of the D1 protein and discuss the difficulties associated with the prediction of new types of inhibitors, since many of the problems involved with enlarged active sites and insertions near the binding region are not restricted to the structure under investigation, but are of more general interest.

2 EXPERIMENTAL

The structures of the compounds synthesized (Table 1) were confirmed by [^{1}H]NMR, recorded at 300 MHz using tetramethylsilane as the internal standard in deuterochloroform or hexadeuterodimethylsulfoxide. The chemical shifts are indicated as δ(ppm) values. The melting points (m.p.) of the compounds are uncorrected.

2.1 SYNTHESIS OF COMPOUNDS

2.1.1 General procedure for the 4-chlorocinnolines

The cinnolines were synthesized (Fig. 2) as described in the literature.[15–17] The appropriately substituted *ortho*-aminophenylbenzylketones were diazotized in hydrochloric acid (1 M). Cyclization of the diazonium compound gave the 4-hydroxy-3-phenyl cinnoline derivatives in 63–89% yield. The 4-chloro derivatives were obtained by treatment with phosphorus pentachloride in phosphorus oxychloride. After the usual workups, the compounds were purified by silica gel column chromatography.

8-methyl-4-chloro-3-phenylcinnoline (**1**): 86% yield; m.p. 103–105°C; [^{1}H]NMR(DMSO) 2·99 (s,3H), 7·61–7·98 (m,7H), 8·16 (d,1H).

4-chloro-8-fluoro-3-phenylcinnoline (**6**): 82% yield, m.p. 157–158°C; [^{1}H] NMR (DMSO) 7·60–7·70 (m,3H), 7·90–8·00 (m,3H), 8·05–8·20 (m,2H).

4-chloro-8-bromo-3-phenylcinnoline (**7**): 88% yield, m.p. 150–151°C; [^{1}H]NMR (DMSO) 7·60–7·70 (m,3H), 7·89–7·98 (m,3H), 8·36–8·42 (d,2H).

4-chloro-7-methyl-3-phenylcinnoline (**8**): 89% yield, m.p. 116–117°C; [^{1}H]NMR (DMSO) 2·68 (s,3H), 7·59–7·75 (m,5H), 7·92 (d,1H), 8·21 (d,1H), 8·39 (s,1H).

Replacement of the 4-chloro atom: In position 4, substituted compounds were obtained by the reaction of the 4-chlorocinnolines with the sodium or potassium salts of the appropriate nucleophile in tetrahydrofuran. After the usual workup the compounds were purified by silica gel column chromatography.

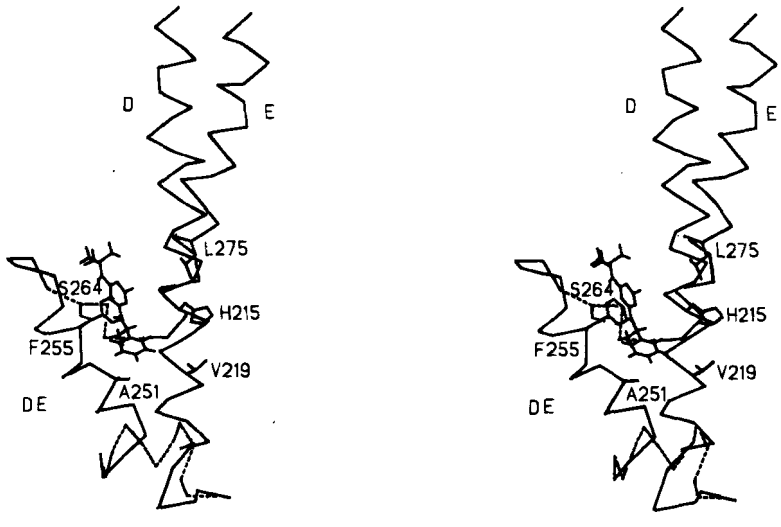

Fig. 1. Stereo presentation of the model of the herbicide binding niche of the D1 protein with compound **22** marking the binding site. Helices D, DE and E are labelled as well as amino acid residues changed in resistant mutants or important as hydrogen bond partner (His215, Val219, Ala251, Phe255, Ser264, Leu275). The residues, which had to be inserted with respect to the photosynthetic reaction centre of *Rps viridis* are drawn in broken lines. In the loop region between helices DE and E all amino acid residues at positions 263–267 are drawn in broken lines.

TABLE 1a
Chemical Structures and IC_{50} Values of the Compounds Investigated

Structure	*Compound*	*R*	*X*	IC_{50} (μM)
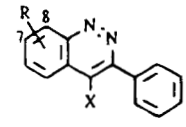	1	$8CH_3$	Cl	0·3
	2	$8CH_3$	OCH_3	1·7
	3	$8CH_3$	SCH_3	3·2
	4	$8CH_3$	OC_6H_5	47·0
	5	$8CH_3$	$COOCH_3$	20·0
	6	8F	Cl	1·6
	7	8Br	Cl	3·9
	8	$7CH_3$	Cl	>100
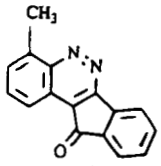	9			3·5
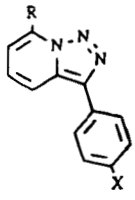	10	CH_3	H	2·3
	11	Br	H	0·024
	12	Cl	H	0·095
	13	OCH_3	H	0·46
	14	SCH_3	H	0·16
	15	$NHN(CH_3)_2$	H	0·47
	16	$Si(CH_3)_3$	H	1·2
	17	Br	C_6H_5	0·18
	18	Br	OC_6H_5	0·085
	19	Br	CH_3	0·065
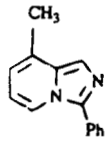	20			>100
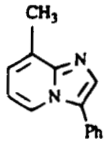	21			0·61

4-methoxy-8-methyl-3-phenylcinnoline (**2**): 84% yield, m.p. 77–78°C; [^{1}H]NMR (DMSO) 2·99 (s,3H), 3·77 (s, 3H), 7·60–8·01 (m,7H), 8·11 (d,1H).

8-methyl-4-methylthio-3-phenylcinnoline (**3**): 63% yield, m.p. 96–97°C; [^{1}H]NMR (DMSO) 2·19 (s,3H), 2·98 (s,3H), 7·59–7·89 (m,7H), 8·32 (d,1H).

8-methyl-4-phenoxy-3-phenylcinnoline (**4**): 64% yield, m.p. 115–116°C; [^{1}H]NMR (DMSO) 3·02 (s,3H), 6·81 (d,2H), 7·00 (t,1H), 7·24 (t,2H), 7·40–7·80 (m,6H), 8·01 (d,2H).

2.1.2 Indeno[1,2-c]cinnoline-11-one

8-Methyl-3-phenylcinnoline-4-carboxylic acid (m.p. 280–300°C) was prepared (Fig. 2) analogously to the description by Baumgarten and Furnas.[18] The acid was then treated with thionyl chloride and the crude material was added to aluminium chloride in dichloroethane and stirred at 80°C for 48 h.[19] After workup and purification (silica gel column chromatography), 3-methyl-indeno[1,2-*c*]cinnoline-11-one (**9**) was obtained in 30% yield. m.p. 220–225°C; [^{1}H]NMR ($CDCl_3$) 2·99 (s,3H), 7·45 (t,1H), 7·56 (d,1H), 7·61–7·77 (m,3H), 8·14 (d,1H), 8·49 (d,1H).

The crude 4-carbonyl chloride was treated with potassium methanolate in tetrahydrofuran. After the workup and purification, methyl 8-methyl-phenylcinnoline-4-carboxylate (**5**) was obtained in 89% yield. m.p. 109–110°C, [^{1}H]NMR ($CDCl_3$) 3·10 (s,3H), 3·83 (s,3H), 7·49–7·90 (m,8H).

TABLE 1b
Chemical Structures and IC_{50} Values of the Compounds Investigated

Structure	*Compound*	*R*	*X*	*n*	IC_{50} (μM)
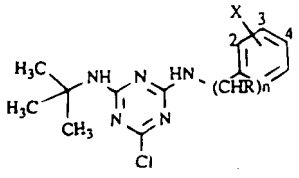	22	(*S*)-CH_3	H	1	1·8
	23	(*R*)-CH_3	H	1	>100
	24	H	H	1	6·0
	25	H	2OCH_3	1	1·5
	26	H	3OCH_3	1	5·4
	27	H	4OCH_3	1	58·0
	28	H	2,6(OCH_3)$_2$	1	>100
	29	H	H	2	2·3
	30	H	H	3	8·1
	31	H	H	4	>100
	32	H	4CH_3	1	26·0

Structure	*Compound*	R^1	R^2	R^3	IC_{50} (μM)
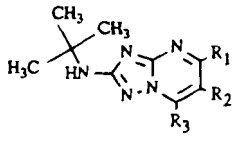	33	H	H	H	23
	34	CH_3	H	H	0·42
	35	CF_3	H	H	0·55
	36	Cl	H	H	0·39
	37	OCH_3	H	H	4·8
	38	C_6H_5	H	H	>100
	39	H	CH_3	H	62·0
	40	CH_3	H	CH_3	18·0
	41	CH_3	CH_3	H	0·26
	42	CH_3	H	OH	17·0
	43	C_2H_5	H	H	14·0
	44	OC_6H_5	H	H	>100
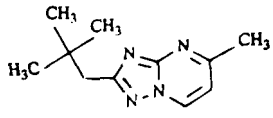	45				>100

2.1.3 1,2,3-triazolo[1,5-a]pyridines

The synthetic route to these compounds is shown in Fig. 3. The 3-phenyl-1,2,3-triazolo[1,5-*a*]pyrimidines were prepared as described by Bower and Ramage.[20] The appropriately substituted phenyl-2-pyridyl ketones and hydrazine hydrate were heated at 100°C for 3 h. On cooling, the solution deposited the hydrazones. This crude material was added to potassium ferricyanide and

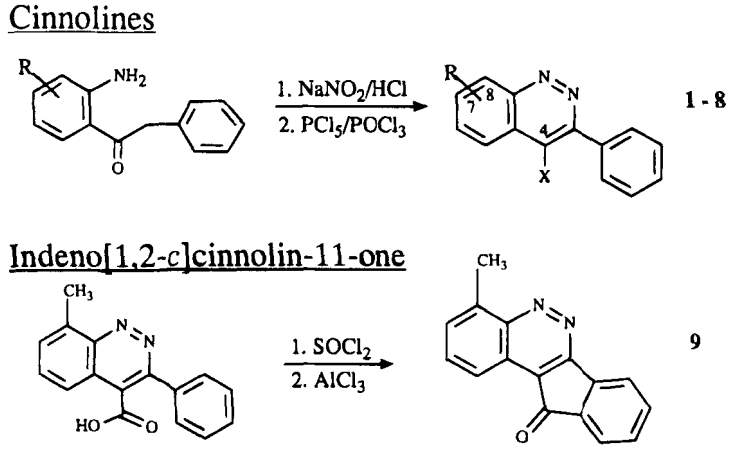

Fig. 2. Synthesis of cinnoline compounds **1–9**.

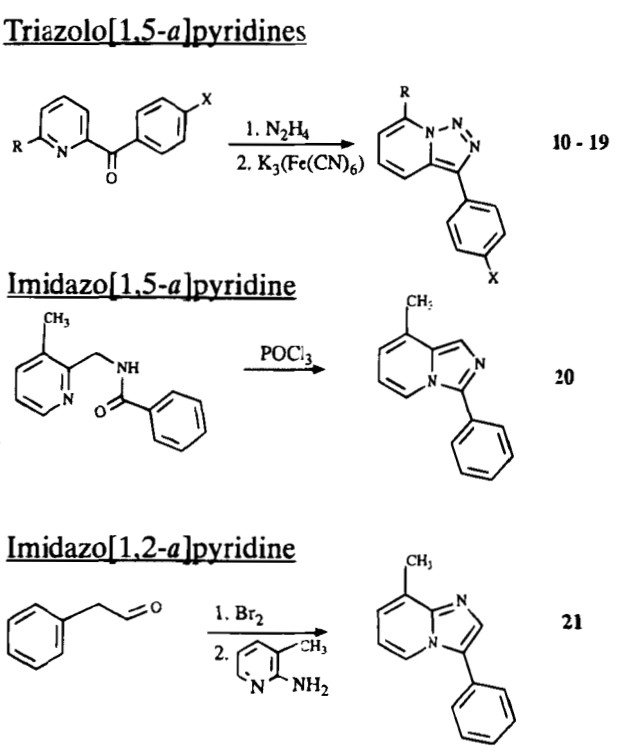

Fig. 3. Synthesis of pyridine compounds **10–21**.

sodium hydrogen carbonate in water and heated at 100°C for 45 min. The usual workup gave crystalline 3-phenyl-1,2,3-triazolo[1,5-*a*]pyridines.

7-methyl-3-phenyl-1,2,3-triazolo[1,5-*a*]pyridine (**10**): 90% yield, m.p. 113–114°C, [^{1}H]NMR ($CDCl_3$)2·93 (s, 3H), 6·82 (d,1H), 7·27 (t,1H), 7·40 (t,1H), 7·52 (t,2H), 7·91 (d,1H), 8·00 (d,2H).

7-chloro-3-phenyl-1,2,3-triazolo[1,5-*a*]pyridine (**12**): 61% yield, m.p. 133–135°C, [^{1}H]NMR ($CDCl_3$)7·10 (d, 1H), 7·30–7·55 (m,4H), 7·95 (m,3H).

The 7-bromo derivatives were prepared from the corresponding 3-phenyl-1,2,3-triazolo[1,5-*a*]pyridines in hexane + toluene (1 + 2 by volume) with butyl lithium at −40°C for 2 h. 1,2-Dibromotetrachloroethane in toluene then was added and the reaction mixture was kept at room temperature for 10 h.[21]

7-bromo-3-biphenyl-1,2,3-triazolo[1,5-*a*]pyridine (**17**): 46% yield, m.p. 193–194°C, [^{1}H]NMR ($CDCl_3$) 7·20–7·52 (m,5H), 7·68 (d,2H), 7·78 (d,2H), 8·05 (m,3H).

7-bromo-3-(4-phenoxyphenyl)-1,2,3-triazolo[1,5-*a*]-pyridine (**18**): 75% yield, m.p. 109–110°C, [^{1}H]NMR ($CDCl_3$) 7·05–7·45 (m,9H), 7·87–8·02 (m,3H).

7-bromo-3-(4-methylphenyl)-1,2,3-triazolo[1,5-*a*]-pyridine (**19**): 83% yield, m.p. 133–135°C, [^{1}H]NMR ($CDCl_3$) 2·42 (s,3H), 7·15–7·30 (m,2H), 7·35 (d,2H), 7·85 (d,2H), 8·00 (d,1H).

In position 7, substituted compounds were obtained by replacement of the 7-bromo atom by appropriate nucleophiles. The reaction was performed in dimethylformamide for 1–20 h at 60–70°C. The usual workup gave the crystalline compounds.

7-methoxy-3-phenyl-1,2,3-triazolo[1,5-*a*]pyridine (**13**): 83% yield, m.p. 136–137°C, [^{1}H]NMR ($CDCl_3$) 4·25 (s,3H), 6·28 (d,1H), 7·25–7·42 (m,2H), 7·51 (t,2H), 7·65 (d,1H), 7·99 (d,2H).

7-methylthio-3-phenyl-1,2,3-triazolo[1,5-*a*]pyridine (**14**): 86% yield, m.p. 138–139°C, [^{1}H]NMR ($CDCl_3$) 2·70 (s,3H), 6·80 (d,1H), 7·25–7·42 (m,2H), 7·85 (d,1H), 7·98 (d,2H).

7-(*N*,*N*-dimethylhydrazino)-3-phenyl-1,2,3-triazolo-[1,5-*a*]pyridine (**15**): 75% yield, m.p. 93–94°C, [^{1}H]NMR ($CDCl_3$) 3·22 (s,6H), 6·28 (d,1H), 7·25–7·42 (m,2H), 7·51 (t,2H), 7·61 (d,1H), 7·98 (d,2H).

7-Trimethylsilyl-3-phenyl-1,2,3-triazolo[1,5-*a*]pyridine (**16**) was obtained from the 7-lithium derivative by reaction with chlorotrimethylsilane: 78% yield, n_D^{20} = 1·5928, analysis: calc. 67·4% C, 6·9% H, 15·7% N, found 67·7% C, 6·8% H, 15·1% N.

All compounds were purified by silica gel column chromatography.

2.1.4 *Imidazo[1,5-a]pyridine*

7-Methyl-3-phenyl-imidazo[1,5-*a*]pyridine (**20**) was prepared by phosphoryl chloride treatment of 2-benzamidomethyl-3-methyl-pyridine.[22,23] Purification by silica gel column chromatography gave the crystalline compound: 46% yield, m.p. 92–94°C, [^{1}H]NMR ($CDCl_3$) 2·48 (s,3H), 6·52 (m,2H), 7·40–7·53 (m,4H), 7·80 (m,2H), 8·15 (m,1H).

2.1.5 *Imidazo[1,2-a]pyridine*

7-Methyl-3-phenyl-imidazo[1,2-*a*]pyridine (**21**) was prepared from 2-amino-3-picoline and bromophenyl acetaldehyde in 1,2-dimethoxyethane at room temperature for 60 h.[24] The usual workup gave the crystalline compound: 53% yield, m.p. 76–77°C, [^{1}H]NMR ($CDCl_3$) 2·68 (s,3H), 6·75 (t,1H), 7·02 (d,1H), 7·38–7·62 (m,5H), 7·70 (s,1H), 8·23 (d,1H).

2.1.6 *Triazines*

The triazines were synthesized (Fig. 4) as described in the literature.[25] 2-*tert*-Butylamino-*s*-triazine was prepared by condensation of *tert*-butylamine and cyanuric chloride in the presence of sodium hydrogen carbonate in acetone at 3–5°C. After the usual workup, the crude product (m.p. 130°C) was condensed with the appropriate amino compound in the presence of potassium carbonate in water + tetrahydrofuran (5 + 3 by volume) at room temperature. All products were purified by silica gel column chromatography.

(*S*)-2-*tert*-butylamino-4-chloro-6-(α-methylbenzyl)-*s*-triazine (**22**): 74% yield; m.p. 110–111°C, [^{1}H]NMR ($CDCl_3$) 1·28 (s,9H), 1·53 (d,3H), 5·08 (qd,1H), 5·30 (s_{br},1H), 5·73 (s_{br},1H), 7·20–7·40 (m,5H).

(*R*)-2-*tert*-butylamino-4-chloro-6-(α-methylbenzyl)-*s*-triazine (**23**): 79% yield, m.p. 105–106°C, [^{1}H]NMR

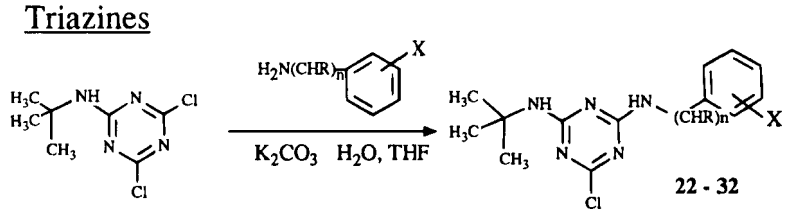

Fig. 4. Synthesis of triazine compounds **22–32**.

(DMSO) 1·20 (s,9H), 1·41 (d,3H), 5·00 (qd,1H), 7·20–7·40 (m,5H), 7·49 (s,1H), 8·41 (d,1H).

2-benzylamino-4-*tert*-butylamino-6-chloro-*s*-triazine (**24**): 46% yield, m.p. 137–139°C, [^{1}H]NMR (DMSO) 1.20 (s,9H), 4·45 (d,2H), 7·10–7·30 (m,5H), 7·52 (s,1H), 8·28 (t_{br},1H).

2-*tert*-butylamino-4-chloro-6-(2-methoxybenzylamino)-*s*-triazine (**25**): 75% yield, m.p. 137–138°C, [^{1}H]NMR (DMSO) 1·20 (s,9H), 3·80 (s,3H), 4·45 (d,2H), 6·83–7·00 (m,2H), 7·10–7·28 (m,2H), 7·50 (s,1H), 8·19 (t_{br},1H).

2-*tert*-butylamino-4-chloro-6-(3-methoxybenzylamino)-*s*-triazine (**26**): 52% yield, m.p. 130–131°C, [^{1}H]NMR (DMSO) 1·20 (s,9H), 3·80 (s,3H), 4·45 (m,2H), 6·76–7·00 (m,2H), 7·10–7·25 (m,2H), 7·50 (s,1H), 8·20 (t_{br},1H).

2-*tert*-butylamino-4-chloro-6-(4-methoxybenzylamino)-*s*-triazine (**27**): 51% yield, m.p. 100–101°C, [^{1}H]NMR (DMSO) 1·30 (s,9H), 3·72 (s,3H), 4·40 (d,2H), 6·87 (m, 2H), 7·20 (m,2H), 7·53 (s,1H), 8·30 (t_{br},1H).

2-*tert*-butylamino-4-chloro-6-(2,6-dimethoxybenzylamino)-*s*-triazine (**28**): 73% yield, m.p. 90–92°C, [^{1}H]NMR (DMSO) 1·41 (s,9H), 3·79 (s,6H), 4·57 (d,2H), 6·65 (m,2H), 7·20–7·30 (m,2H), 7·45 (s,1H).

2-*tert*-butylamino-4-chloro-6-(2-phenylethylamino)-*s*-triazine (**29**): 45% yield, m.p. 200–202°C, [^{1}H]NMR (DMSO) 1·35 (s,9H), 2·60 (t,2H), 3·27 (m,2H), 7·12–7·32 (m,5H), 7·51 (s,1H), 7·85 (t_{br},1H).

2-*tert*-butylamino-4-chloro-6-(3-phenylpropylamino)-*s*-triazine (**30**): 88% yield, m.p. 136–137°C, [^{1}H]NMR (DMSO) 1·35 (s,9H), 1·80 (m,2H), 2·61 (t,2H), 3·25 (m, 2H), 7·12–7·30 (m,5H), 7·50 (s,1H), 7·90 (t_{br},1H).

2-*tert*-butylamino-4-chloro-6-(4-phenylbutylamino)-*s*-triazine (**31**): 98% yield, m.p. 95–96°C, [^{1}H]NMR (DMSO) 1·32 (s,9H), 1·45–1·65 (m,4H), 2·60 (t_{br},2H), 3·25 (m,2H), 7·10–7·30 (m,5H), 7·50 (s,1H), 7·80 (t_{br},1H).

2-*tert*-butylamino-4-chloro-6-(4-methylbenzylamino)-*s*-triazine (**32**): 87% yield, m.p. 117–118°C, [^{1}H]NMR (DMSO) 1·27 (s,9H), 2·27 (s,3H), 4·44 (d,2H), 7·07–7·20 (m,4H), 7·53 (s,1H), 8·32 (t_{br},1H).

2.1.7 Triazolo[1,5-a]pyrimidines

The synthetic route is shown in Fig. 5. The starting material for the 2-*tert*-butylamino-1,2,4-triazolo[1,5-*a*]-pyrimidines, 3-amino-5-*tert*-butylamino-1,2,4-triazole, was prepared in 85% yield (m.p. 155°C) following the procedure of Reiter *et al.*[26,27] The latter compound was suspended in toluene and the appropriately substituted 1,3-dicarbonyl compound and *para*-toluenesulfonic acid were added. After the addition was complete, the solution was stirred at room temperature for 16 h. After evaporation under vacuum, a crystalline solid was obtained. The crude products were recrystallized from diisopropylether.

2-*tert*-butylamino-1,2,4-triazolo[1,5-*a*]pyrimidine (**33**): 69% yield, m.p. 164–165°C, [^{1}H]NMR (DMSO) 1·40 (s,9H), 6·72 (s_{br},1H), 7·00 (t,1H), 8·50 (d,1H), 9·02 (d,1H).

2-*tert*-butylamino-5-methyl-1,2,4-triazolo[1,5-*a*]pyrimidine (**34**): 97% yield, m.p. 165–167°C, [^{1}H]NMR (DMSO) 1·40 (s,9H), 2·51 (s,3H), 6·60 (s_{br},1H), 6·89 (d,1H), 8·82 (d,1H).

2-*tert*-butylamino-6-methyl-1,2,4-triazolo[1,5-*a*]pyrimidine (**39**): 54% yield, m.p. 188–189°C, [^{1}H]NMR (DMSO) 1·39 (s,9H), 2·29 (s,3H), 6·59 (s_{br},1H), 8·39 (s,1H), 8·89 (s,1H).

2-*tert*-butylamino-5,7-dimethyl-1,2,4-triazolo[1,5-*a*]-pyrimidine (**40**): 49% yield, m.p. 203–204°C, [^{1}H]NMR (DMSO) 1·40 (s,9H), 2·43 (s,3H), 2·58 (s,3H), 6·59 (s_{br},1H), 6·80 (s,1H).

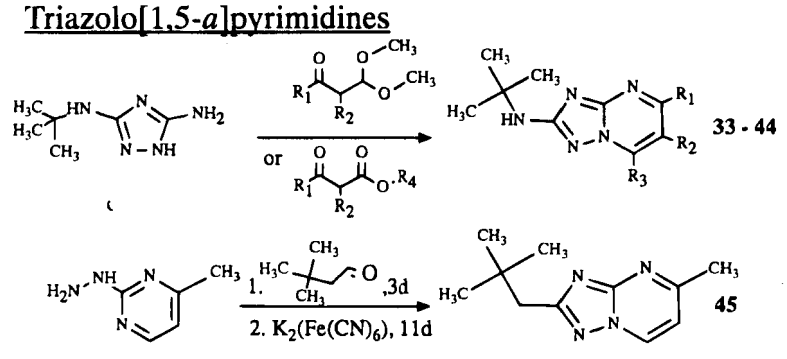

Fig. 5. Synthesis of triazolo[1,5-*a*]pyrimidines **33–45**.

2-*tert*-butylamino-7-hydroxy-5-methyl-1,2,4-triazolo-[1,5-*a*]pyrimidine (**42**): 93% yield, m.p. > 300°C, [^{1}H]NMR (DMSO) 1·35 (s,9H), 2·25 (s,3H), 5·62 (s_{br},1H), 6·21 (s,1H), 12·67 (s_{br},1H).

The 5-chloro compound (**36**) was prepared from the 5-hydroxy derivative by treatment with phosphorus oxychloride.

2-*tert*-butylamino-5-chloro-1,2,4-triazolo[1,5-*a*]pyrimidine (**36**): 93% yield, m.p. 135–136°C, [^{1}H]NMR (DMSO) 1·40 (s,9H), 6·93 (s_{br},1H), 7·10 (d,1H), 9·04 (d, 1H).

Replacement of the 5-chloro atom: 5-substituted compounds were obtained by the reaction of the 5-chlorotriazolo[1,5-*a*]pyrimidine with the sodium salt of the appropriate nucleophile in tetrahydrofuran. After the workup, the compounds were purified by silica gel column chromatography.

2-*tert*-butylamino-5-methoxy-1,2,4-triazolo[1,5-*a*]-pyrimidine (**37**): 90% yield, m.p. 150–151°C, [^{1}H]NMR (DMSO) 1·39 (s,9H), 3·92 (s,3H), 6·39 (s_{br},1H),6·45 (d, 1H), 8·26 (d,1H).

2-*tert*-butylamino-5-phenoxy-1,2,4-triazolo[1,5-*a*]-pyrimidine (**44**): 64% yield, m.p. 166–167°C, [^{1}H]NMR (DMSO) 1·38 (s,9H), 6·41 (s_{br},1H), 6·69 (d,1H), 8·91 (d, 1H), 7·25–7·52 (m,5H). Some compounds were obtained by dehalogenation of the appropriately substituted 7-chloro derivatives.[28] The latter compounds were prepared from the 7-hydroxy derivatives as described above.

2-*tert*-butylamino-5-trifluoromethyl-1,2,4-triazolo[1,5-*a*]pyrimidine (**35**): 42% yield, m.p. 139–140°C, [^{1}H]NMR (DMSO) 1·41 (s,9H), 7·22 (s_{br},1H),7·46 (d, 1H), 9·31 (d,1H).

2-*tert*-butylamino-5-phenyl-1,2,4-triazolo[1,5-*a*]pyrimidine (**38**): 80% yield, m.p. 180–181°C, [^{1}H]NMR (DMSO) 1·41 (s,9H), 6·71 (s_{br},1H), 7·55–8·20 (m,5H), 7·60 (d,1H), 9·05 (d,1H).

2-*tert*-butylamino-5,6-dimethyl-1,2,4-triazolo[1,5-*a*]-pyrimidine (**41**): 58% yield, m.p. 229–230°C, [^{1}H]NMR (DMSO) 1·37 (s,9H), 2·21 (s,3H), 2·42 (s,3H), 8·76 (s,1H).

2-*tert*-butylamino-5-ethyl-1,2,4-triazolo[1,5-*a*]pyrimidine (**43**): 78% yield, m.p. 132–134°C, [^{1}H]NMR (DMSO) 1·26 (t,3H), 1·40 (s,9H), 2·79 (q,2H), 6·58 (s_{br},1H), 6·90 (d,1H), 8·89 (d,1H).

The synthesis of the 2-alkyl derivative was based on a Dimroth-like rearrangement of triazolo[4,3-*a*]pyrimidines to the isomeric [1,5-*a*] series.[29] We used as starting material 2-hydrazino-4-methylpyrimidine, which was condensed with 3,3-dimethylbutyraldehyde. This crude hydrazone was added to potassium ferricyanide in methanol + water (1 + 4 by volume) and stirred for 11 days at room temperature. After the usual workup, the compound was purified by silica gel column chromatography. 2-(2,2-Dimethylpropyl)-5-methyl-1,2,4-triazolo[1,5-*a*]pyrimidine (**45**): 8% yield, m.p. 98–99°C, [^{1}H]NMR (DMSO) 1·00 (s,9H), 2·60 (s,2H), 7·20 (d,1H), 9·19 (d,1H).

2.2 Biological data

The inhibitory action of herbicides was determined in triplicate assays. At least five different concentrations of each compound were used to inhibit the electron transport between 20 and 80%. The results were plotted in a dose–response curve and linearized by log/logit transformation from which IC_{50} values were derived. The IC_{50} value is the concentration of herbicide which inhibits half maximal photosystem II electron transport. Photosystem II electron transport was measured at 25°C in a microtiter plate assay using saturating light. Ferricyanide (1 mM) was used as an artificial electron acceptor. Evolved ferricyanide was complexed with 1,10-phenanthroline to produce a chromogen that was detected at 515 nm. In a total volume of 100 µl, the assay medium consisted of tricine, 25 mM pH 7·8; disodium hydrogen phosphate, 5 mM; magnesium chloride, 5 mM; ammonium chloride, 2·5 mM and broken pea chloroplasts with a total chlorophyll content of 5·4 µg. Under such conditions linear amounts of ferricyanide were produced up to 10 min. After illumination for 5 min, the reaction was terminated by addition of trichloroacetic acid (67·5 ml litre^{-1}, 25 µl). Finally, 200 µl of a solution of sodium acetate 1·125 M; citrate, 62 mM; iron(III) chloride, 0·22 mM; acetic acid, 7·9 mM and 1,10-phenanthroline, 3·8 mM was added. After 3 min incubation, the absorbance at 515 nm was measured in a microplate reader. Chloroplasts from peas were prepared according to Latzko and Gibbs.[30] Prepared chloroplasts were frozen at −20°C and thawed directly before use.

For the mutant D1 proteins, the chloroplasts were isolated from the green alga *Chlamydomonas reinhardtii*. Since the sequence homology between the D1 proteins of this alga and that of e.g. spinach is 93%, the alga has often been used for the determination of IC_{50} values. Where mutant data were available, it was advantageous to use the ratio of IC_{50} values of resistant and susceptible (i.e. wild type) species (R/S). The R/S values of the commonly used five mutants of the D1 protein of *C. reinhardtii* were kindly provided by Prof. A. Trebst (University Bochum) and are listed in Table 2.

2.3 Computational methods

All modelling was done using the molecular modelling package InsightII (Biosym Technologies, Inc.). The initial model of the active site of the D1 protein is described in detail by Egner *et al.*[9] Ligands were manually adjusted into the active site with hydrogen bonds either to the hydroxyl group of Ser264, the peptide NH of Phe265 or the side chain of His215. Additionally, the ligands were accommodated into the binding niche in such a way that their chemical groups superimposed

TABLE 2
R/S Values of Some of the Compounds Investigated

Compound	*Val 219-Ile*	*Ala 251-Val*	*Phe 255-Tyr*	*Ser 264-Ala*	*Leu 275-Phe*
7	63	10	0·1	10	3
11	3	50	0·3	100	3
34	40	>126	1	40	>126
41	5	>16	0·3	8	10
Atrazine	2	25	16	160	1

IC_{50} values were measured at mutant proteins of *Chlamydomonas reinhardtii* and converted to R/S values. The data for atrazine are taken from Tietjen *et al.*[34]

with energetically favourable binding sites for probe groups (methyl group, amine nitrogen, sulfur, carbonyl and hydroxyl oxygens) as determined with the program Grin and Grid.[31] The protein–ligand complexes were relaxed with energy minimizations. The calculations were performed with Discover 2.8, applying the consistent valence force field (Biosym Technologies, Inc.) on a Siemens supercomputer S200 using a protocol previously described.[9] The automatic parameter assignment reproduced sufficiently the bond lengths and angles found in crystal structures of related compounds. The interaction energy E between a ligand and the protein was calculated with the energies defined as

$$E = E_{PL} - (E_P + E_L)$$

E_{PL} being the energy of the protein–ligand complex, E_P that of the protein and E_L that of the ligand. The energy of the protein and the ligand was determined in the conformation these molecules adopt in the protein–ligand complex. The interaction energy in combination with the goodness of fit of a compound within the binding niche and the results from mutagenesis studies were used as a guide to estimate the relative in-vitro activities. The area of the herbicide binding niche where inhibitors could be accommodated was calculated with the program Cavity[32] and visualized with Insight (Biosym Technologies, Inc.) or SHELXTL + (Siemens Analytical X-ray Instruments, Inc.).

3 RESULTS AND DISCUSSION

3.1 Synthesis of compounds

In our work we chose new fused heterocyclic compounds to obtain novel information on the interaction between the inhibitors and the herbicide binding niche of the D1 protein. From the synthetic point of view, important criteria for the selection of compounds were a simple way of preparation and the possibility of significantly varying the substituents. For all compound classes investigated, the synthesis of the heterocyclic skeleton was known in the literature, but the specific substitution patterns are described for the first time.

The cinnolines were synthesised (Fig. 2) starting with appropriately substituted *ortho*-aminophenylketones.[15–17] Substituents were primarily varied in positions 4 and 8 (see Table 1a). The compounds were obtained in 63 to 89% yields and the in-vitro activities were in the range of 0·3 μM to >100 μM. The 4-carboxylic acid derivative which was prepared according to Baumgarten and Furnas[18] was cyclized to the indeno[1,2-*c*]cinnoline-11-one in 30% yield.

The synthetic routes to the 1,2,3-triazolo[1,5-*a*]pyridines, the imidazo[1,5-*a*]pyridines and the imidazo[1,2-*a*]pyridines are shown in Fig. 3. The 3-phenyl-1,2,3-triazolo[1,5-*a*]pyridines were prepared as described by Bower and Ramage in yields between 61 and 90%, starting with appropriately substituted phenyl-2-pyridyl ketones.[20] The 7-bromo derivatives were prepared from the appropriate 7-lithium-1,2,3-triazolo[1,5-*a*]pyridines by reaction with 1,2-dibromotetrachloroethane, with yields between 46 and 83%. Other substituents at the 7-position, such as methoxy or methylthio, were obtained in 75 to 86% yield by replacement of the 7-bromo atom. Starting with 2-benzamido-methyl-3-methylpyridine or 2-amino-3-picoline the 7-methyl-3-phenylimidazo[1,5-*a*]-pyridines and [1,2-*a*]-pyridines were obtained.

The triazines were synthesized following a published procedure.[25] First we prepared the 2-*tert*-butylamino-*s*-triazine and then the other appropriately substituted amino group was introduced (Fig. 4). The yields for the triazines were in the range of 45 to 98% and the IC_{50} values varied over two orders of magnitude.

The synthesis of the 2-*tert*-butylamino-1,2,4-triazolo[1,5-*a*]pyrimidines is shown in Fig. 5. The 3-amino-5-*tert*-butylamino-1,2,4-triazole was prepared in 85% yield following a procedure of Reiter.[27] In a condensation step with the appropriately substituted 1,3-dicarbonyl compounds, the 5-, 6- and 7-substituted 2-*tert*-butylamino-1,2,4-triazolo-[1,5-*a*]-pyrimidines were obtained with yields of 42 to 97%. The best IC_{50} values were determined to be 0·26 (**41**) and 0·42 μM (**34**). The synthesis of the 2-alkyl derivative is based on the Dimroth-like rearrangement of the isomeric triazolo[4,3-*a*]-pyrimidines. We used 2-hydrazino-4-methylpyridine as starting material, which was transformed to

the corresponding hydrazone, cyclized and isomerized with ferricyanide to the 2-(2,2-dimethylpropyl) derivative in 8% yield.

3.2 Modelling results

The starting point for our present investigation was the structure of the herbicide binding niche of the D1 protein derived from homology modelling using the bacterial photosynthetic reaction centre of *Rps viridis*. It should be emphasized that the basic assumption of homology studies is that the three-dimensional structure of proteins with comparable functionality is conserved even if the sequence homology is low. Since the model has already been described in detail,[9] only a short introduction is given here. The model consists of 97 amino acid residues building up three helices named D, DE and E in analogy to the bacterial structure (Fig. 1). Conserved functional amino acid residues indicated that the loops connecting the helices had to be modified: 14 additional amino acid residues had to be added between helices D and DE and three residues between helices DE and E. The orientations of the helices and the conformation of the loops in our model were chosen so that the positions of His215 and Ser264, the main hydrogen-bond donors and acceptors for inhibitors in the binding niche, were similar with regard to the bacterial protein. The initial model, supported by mutant data, was already good enough to explain binding properties for at least some members of well-characterized inhibitor classes. Nevertheless, the low homology between the D1 protein and the corresponding bacterial subunit implied that further refinement of the model was necessary in order to utilize it in the de-novo design of herbicides.

3.2.1 Validation of the initial model

To test our initial model, inhibitors were fitted into the active site and the modelling results compared to experimental data. To begin with, we focused our attention on the cinnoline family, a small, well-characterized inhibitor class. For the limited number of cinnolines synthesized it seemed likely that we would find a relationship between binding properties within the active site and in-vitro IC_{50} values. Unfortunately, all cinnolines under investigation (**1–9**, Table 1a) were too small to be unambiguously fitted into the binding niche. Altogether, four different orientations had to be considered as depicted in Fig. 6 in the case of compound **6**. In two of the proposed binding modes, the inhibitors accept a hydrogen bond from His215, in the other two orientations Ser264 is involved as hydrogen-bond donor. Without additional experimental data, it is impossible to decide which amino acid residue interacts with the ligand.

To overcome this difficulty, we thought that IC_{50} values from mutant D1 proteins for the inhibitors

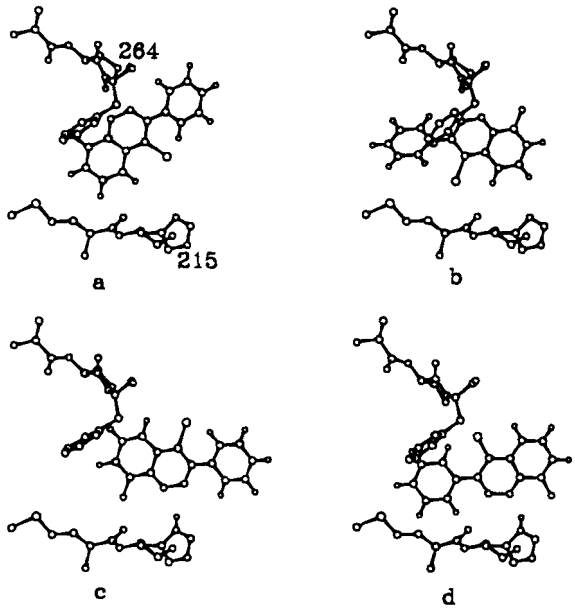

Fig. 6. Four different orientations of compound **6** in the refined model; the orientation of the model is the same as in Fig. 8. a,b: hydrogen bond between Ser264 and the compound; c,d: hydrogen bond between His215 and the compound.

studied could be helpful.[33] Since the D1 proteins of plants and alga are highly homologous, five different mutations in the vicinity of the active site of the protein from the alga *C. reinhardtii* were used to analyze the effects on the binding of the ligands (Table 2). With one of these mutants, Ser264-Ala, the influence of the serine hydroxy group upon inhibitor binding can be investigated. The relatively low R/S value of 10 for compound **7** is indicative of a minor influence of Ser264 and, therefore, makes a hydrogen bond between this residue and the inhibitor unlikely. This already excludes two of the above mentioned possible binding modes (Figs 6a, b). In the other two orientations, His215 acts as a hydrogen bond donor. Since this residue is essential for the coordination of the non-heme iron atom, any replacement of this histidine would severely disturb the function of PS II and give no information concerning contacts between the protein and a ligand. Therefore, the effect of the mutation Val219-Ile was studied, since residues 215 and 219 have well-defined positions in helix E. No conformational changes within the active site are expected upon mutation of Val219, and the sterically demanding Ile219 in the mutant protein is thought to interfere with the hydrogen bond between His215 and an inhibitor. The high R/S value of 63 for compound **7** indicates that, in fact, His215 acts as a hydrogen-bond donor for cinnolines. Nevertheless, it is still impossible to distinguish between the two remaining binding modes (Figs 6c, d) even if inactive compounds like **8**, compounds with enlarged substituents in position X (**2–4**) or annelated compounds like **9** are considered. To identify unambiguously the binding mode for the cinnolines, more experimental data were needed. Since the IC_{50} values of

the cinnolines are only moderate, we decided to concentrate our efforts on a more active class of inhibitors, the triazolopyridines.

The major advantage of the triazolopyridines is that their in-vitro activity covers a broad range from inactive to highly potent (10^{-8} M), which facilitates the interpretation of data (Table 1, **10–21**). As the volumes of the triazolopyridine and cinnoline skeletons are similar, the above-mentioned problems with multiple binding modes were again expected. Our modelling studies with compounds **10–14** indeed revealed four different binding modes comparable to those of the cinnolines. In contrast to the cinnolines, mutant data showed that Ser264 is necessary for the binding of triazolopyridines (Table 2), which reduces the number of binding modes to two (analogous to Figs 6a,b). To determine which of the nitrogen atoms of the triazolopyridine skeleton interacts with the protein, compounds **20** and **21** were synthesized (Table 1). Their IC_{50} values (0·6 and 100 μM) strongly suggest that only the nitrogen atom beside the bridgehead carbon atom functions as hydrogen-bond acceptor.

To reduce further the number of binding modes, the bulky trimethylsilyl moiety was introduced in position R (**16**). In our model, compound **16** could only be accommodated with R pointing towards Ile259, at the C-terminal end of helix DE. Using the unambiguous orientation of compound **16** as a working hypothesis for a binding mode for all triazolopyridines (while keeping in mind that small triazolopyridines may not necessarily adopt only one binding mode), compounds with elongated substituents in the *para* position of the phenyl ring (e.g. compounds **17–19**) could easily be fitted into the binding niche and the IC_{50} values for several inhibitors of this family explained qualitatively. For others (e.g. **15**) predictions were difficult to make and we concluded that the initial model had to be improved. If IC_{50} values are used to derive conclusions about the architecture of the model, a broad variety of inhibitors belonging to the same family and adopting only *one* single binding mode is a prerequisite. Since the synthetic effort in case of the triazolopyridines would have been too high, we focused our interest on the triazines, where new substituents could be easily introduced into the triazine ring.

3.2.2 *Refinement of the model*

The triazine compounds form a well-characterized herbicide family with in-vitro activities ranging over three orders of magnitude, thus facilitating the interpretation of effects caused by different substituents. Several authors have used stereospecific inhibitors of this family to test their models of the D1 protein.[11,34] However, they used compounds with small substituents so that—in our opinion—an ambiguity in binding modes causing problems similar to those that we encountered with the cinnolines and triazolopyridines cannot be ruled out. In contrast to this approach, we chose to study only triazines with a *tert*- butylamino moiety (Table 1b, **22–32**). In the initial model, molecules carrying this bulky substituent can only be fitted into the binding niche in the orientation shown in Fig. 7. The orientation shown in Fig. 7 is in good agreement with experimental data showing that symmetric triazines carrying two *tert*-butylamino groups are inactive.[35] Furthermore the binding position is similar to the crystallographically determined orientation of terbutryn (2-ethylamino-4-*tert*-butylamino-6-methylthio-*s*-triazine) in complex with the bacterial reaction centre *Rps viridis* with two hydrogen bonds between the triazine and the protein, one between the NH of the ethylamino substituent of terbutryn and the hydroxyl group of Ser216 (equivalent to Ser264 in the D1 protein), the other between the triazine ring and the peptide NH of Ile217 (corresponding to Phe265 in the D1 protein).[6] The unambiguous binding mode achieved by the single *tert*-butylamino moiety allowed us to investigate the impact of varying substituents on the triazine ring on the binding properties of the respective inhibitors and thus to draw conclusions concerning the architecture of the binding niche in that area (region A, see Fig. 8).

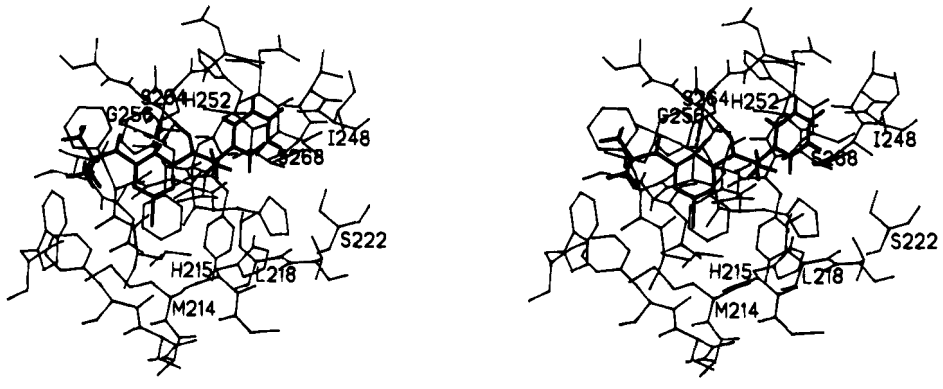

Fig. 7. Stereo presentation of the orientation of compound **22** (in bold) in the herbicide binding niche of the refined model of the D1 protein. The *tert*-butylamino group is pointing to the surface of the D1 protein, the benzylamino moiety is surrounded by the side chains of Leu218, Ile248, His252, Ser268 and Leu271. This area will be called region A within this paper, see also Fig. 8.

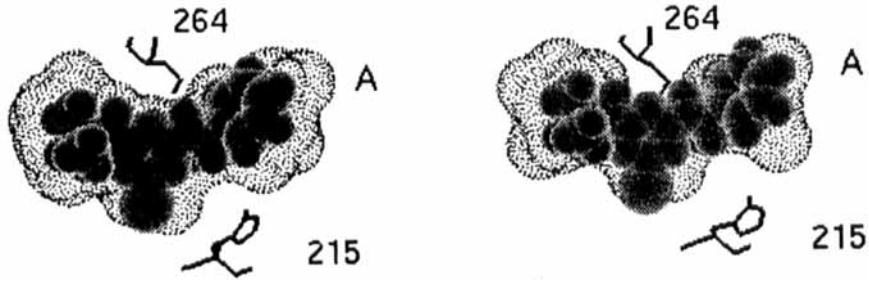

Fig. 8. Comparison of the initial (left) and the refined (right) herbicide binding niche of the D1 protein. Compound **22** is shown with a CPK surface, its benzylamino moiety is pointing in region A (the right side of the figure). For calculation of this presentation of the binding niche see Section 2.3.

Studying the enantiopure compounds **22** and **23** proved to be of special interest as only the (*S*)-isomer is active.[36] This could not be explained with the initial model, as both structures could be accommodated in the binding niche without steric interference with the protein. The model therefore had to be modified so that the (*R*)-isomer could not be fitted into the binding niche, i.e. the area occupied only by the (*R*)-isomer had to be reduced. This was achieved by shifting the *N*-terminus of helix DE towards helix D without affecting the relative distance between Ser264 and His215, and by reorienting residues 267 and 268. After these two modifications, the differences in the IC_{50} values of both isomers could be explained.

To check this improved model, several other triazine derivatives with expected good hydrophobic and hydrophilic interactions in region A were designed. With the help of interaction energies and the steric fit of the compounds, the ligands could be clustered into three groups representing compounds with low, moderate or high IC_{50} values. For many of the compounds, these estimations of relative activities were in good agreement with the later-determined experimental IC_{50} values. For instance, according to the estimations, a compound with one *ortho*-substituent at the benzylamino moiety is active (**25**, $IC_{50} = 1{\cdot}5$ μM), whereas inhibitors with two *ortho*-substituents are too big to fit in the binding niche and are inactive (**28**, $IC_{50} > 100$ μM). In this model there is ample space in the vicinity of the *meta* and *para* positions of the benzylamino moiety. In the bacterial protein, this region is occupied by a small part of an adjacent protein, the H-subunit, for which no equivalent is known in PS II.[37] Therefore, we synthesized several compounds to analyze further the topography of this area. The maximum size of a *meta*-substituent was determined to be that of a methoxy group (**26**, $IC_{50} = 5{\cdot}4$ μM); the same moiety in the *para* position reduced the activity by a factor of ten (**27**, $IC_{50} = 58$ μM). Consequently, further modifications had to be introduced into the model: (1) The side chain of His252 was oriented to point towards the active site and (2) two water molecules were added, making well-defined hydrogen bonds to adjacent amino acid residues. In the absence of a protein equivalent to the bacterial H-subunit, they function as a cover limiting the binding niche in that area. Taken together, these alterations reduced the volume of the binding niche by about 20% in comparison to our initial model (Fig. 8). This refined model was then submitted to energy minimizations, resulting in a structure with comparable energy to the initial model.

With the refined model, a variety of triazines were fitted into the active site and the ranking of their activities estimated. A comparison with in-vitro data showed the quality of our model and its usefulness with respect to these qualitative predictions. Under the assumption that compounds with a longer spacer between the two ring systems occupy a region similar to that described for phenmedipham (methyl *N*-[3-[*N*-methylphenyl)carbamoyloxy]phenyl]carbamate), even the relative rankings of triazines carrying phenethyl-, phenpropyl- or phenbutyl substituents (**29**–**31**) were in good agreement with the modelling results.[9]

3.2.3 De-novo design

The promising results with the triazines encouraged us to test whether the refined model could be used to design a new inhibitor class. As a first step, we directed our attention to compounds with molecular characteristics similar to those of the triazine family. We decided to keep the two nitrogen atoms of the triazines involved in hydrogen bonds to the protein as well as the *tert*-butylamino moiety thereby conserving the binding mode described for the triazines. The triazolopyrimidines contain the required nitrogen atoms, although, in contrast to the triazines, both of them have to function as hydrogen-bond acceptors (Table 1, Fig. 9). Since differing substituents, including the *tert*-butylamino group, can easily be introduced into the triazolopyrimidine skeleton, we chose this family to develop new inhibitors for the D1 protein. Compound **33** was synthesized, subjected to in-vitro tests and found to be a moderately good inhibitor ($IC_{50} = 23$ μM) despite being a relatively simple structure! This result encouraged us to optimize the binding by variation of substituents in position R1. This led to the synthesis of e.g. **34**, **38** and **43**, the most active being **34** with $IC_{50} = 0{\cdot}42$ μM (with respect to substituents in position R1). If a methyl group is added in position R2 (**41**), the IC_{50}

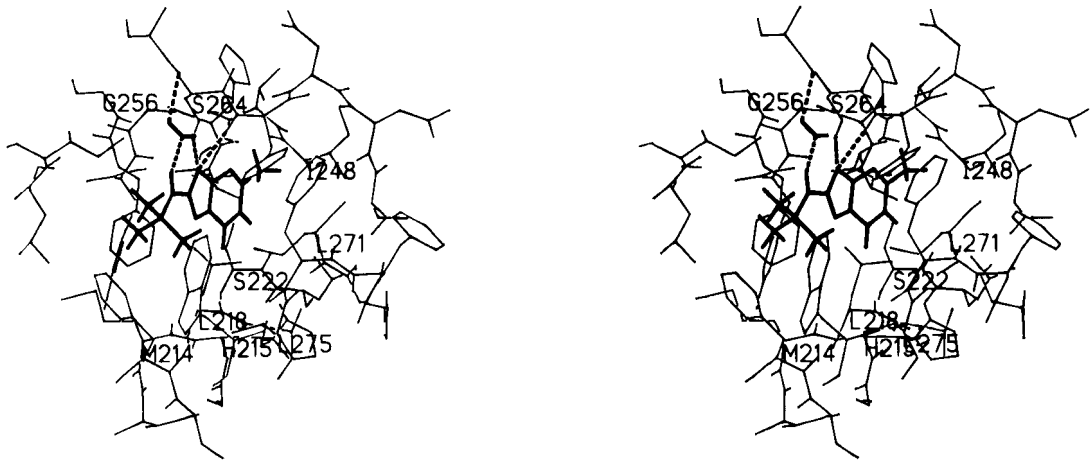

Fig. 9. Stereo presentation of the proposed binding mode of compound **34** involving a water molecule within the refined binding niche of the D1 protein. The ligand and the water molecule are drawn in bold.

value of the compound is even better (0·26 μM). This *in-vitro* activity is comparable to that of commercially important herbicides for the D1 protein like atrazine (6-chloro-N^2-ethyl-N^4-isopropyl-1,3,5-triazine-2,4-diamine; IC_{50} = 0·5 μM). We had thus achieved our aim to design a new class of highly active inhibitors.

Nevertheless, a closer inspection of the in-vitro activity revealed that some results could not be explained by assuming similar binding positions for the triazines and the triazolopyrimidines. Evidence for such a difference was supplied by the IC_{50} values of triazolopyrimidines with a phenyl (**38**) or a phenoxy (**44**) group in position R1. Both compounds turned out to be inactive whereas the corresponding triazines (**24** and **29**) have IC_{50} values of 6 and 2·3 μM, respectively. To scrutinize the differences in binding behaviour, mutant data for both inhibitor classes were carefully analyzed. The mutations of Ser264-Ala and Ala251-Val affect the binding of both inhibitor classes. The effect of the former is more pronounced in the case of a triazine molecule (R/S = 160 for atrazine and 40 for **34**), while the latter mutation greatly influences the binding of **34** (R/S > 126 and 25 for atrazine, Table 2). Surprisingly, mutation Leu275-Phe had a strong impact on **34** (R/S > 126). To the best of our knowledge, this is the first inhibitor to be in close contact with Leu275. A binding mode for **34** accounting for these mutant data is depicted in Fig. 9. The hydrogen bonds between the nitrogen atoms of the triazolopyrimidine skeleton and Ser264 are formed as expected. The *tert*-butylamino substituent is in close contact to Leu275. A water molecule bridges this amino group and the carbonyl oxygen of Ala263, thus explaining the inactivity of **45**, which cannot form this hydrogen bond (Table 1). A pronounced difference is observed in the mutant data of compounds **34** and **41**, which only differ in a methyl group in position R2. The differences in the mutant data can be explained with a slight reorientation of **41** within the binding niche. The position of this compound is shifted and rotated towards Leu271, resulting in an increased distance to Ala251 and Leu275. The hydrogen bonds to the peptide NH of Phe265 and to the water molecule are maintained, but not to the Ser264 side chain, thus explaining the mutant data (less effect of Ala251 and Ser264). As the distance between **41** and Leu275 is increased, a smaller impact of the mutation was indeed expected but not as pronounced as observed.

With the triazolopyrimidines we have found a new potent inhibitor class for the D1 protein. Most of our assumptions concerning the binding properties were supported by experimental data, according for the improved quality of our refined model of the binding niche. Nevertheless, even with a good model, unexpected features such as the orientation of the *tert*-butylamino group of **34** can be observed. This demonstrates the importance of biological data, especially in the prediction and development of new compounds.

4 CONCLUSIONS

In this study we have presented the validation and subsequent refinement of our initial model of the herbicide binding niche of the D1 protein belonging to photosystem II of plants. The major problem during the refinement process was caused by the occurrence of multiple binding modes for small ligands. This could be overcome by the synthesis of compounds with bulky substituents and the analysis of IC_{50} values of mutant D1 proteins. The combined efforts of synthetic chemistry, molecular biology and theoretical chemistry have led to an improved model of the herbicide binding niche with a decreased volume compared to the starting model. Using this refined model, the relative in-vitro activity of inhibitors belonging to different chemical classes has been satisfactorily explained.

Photosystem II has recently been crystallized and it will be interesting to compare our model with the

experimentally determined three-dimensional structure.[38,39] Unfortunately, due to the complexity of the problem, the high resolution structure will not be available in the near future. However, the usefulness of our model in its present state has been demonstrated by the successful de-novo design of inhibitors belonging to the triazolopyrimidine family.

ACKNOWLEDGEMENT

We would like to thank Dr J. Geisler for providing compound **11** and Prof. A. Trebst for providing IC_{50} values for the mutant D1 proteins. We also thank Dr U. Eder for his encouragement and support. The excellent technical assistance of I. Sprung is acknowledged. We are greatly indebted to Dr Anke Müller-Fahrnow and Dr Philip Dudfield for reading the manuscript.

REFERENCES

1. Trebst, A., The topology of the plastoquinone and herbicide binding peptides of Photosystem II in the thylakoid membrane. *Z. Naturforsch.*, **41C** (1986) 240–5.
2. Michel, H. & Deisenhofer, J., Relevance of the photosynthetic reaction center from purple bacteria to the structure of Photosystem II. *Biochemistry*, **27** (1988) 1–7.
3. Barber, J., Rethinking the structure of photosystem two reaction center. *Trends Biochem. Sci.*, **12** (1987) 321–6.
4. Vorpagel, E. R., Molecular modeling: A tool for designing crop protection chemicals. In *Pesticides Minimizing the Risks*, ed. N. N. Ragsdale & R. J. Kuhr. American Chemical Society, Washington, DC, 1987, pp. 115–26.
5. Michel, H., Epp, O. & Deisenhofer, J., Pigment–protein interactions in the Rps. viridis reaction center. *EMBO J.*, **5** (1986) 2445–51.
6. Michel H., Weyer, K. A., Gruenberg, H., Dunger, I., Oesterhelt, D. & Lottspeich, F., The 'light' and 'medium' subunits of the photosynthetic reaction centre from *Rhodopseudomonas viridis:* isolation of genes, nucleotide and amino acid sequence. *EMBO J.*, **5** (1986) 1149–58.
7. Sinning, I., Michel, H., Mathis, P. & Rutherford, W. A., Terbutryn resistance in a purple bacterium can induce sensitivity toward the plant herbicides DCMU. *FEBS Lett.*, **256** (1989) 192–4.
8. Allen, J. P., Feher, G., Yeates, T. O., Komiya, H. & Rees, D. C., Structure of the reaction center from Rhodobacter sphaeroides R-26: The protein subunits. *Proc. Natl Acad. Sci. USA*, **84** (1987) 6162–6.
9. Egner, U., Hoyer, G.-A. & Saenger, W., Modeling and energy minimization studies on the herbicide binding protein (D1) of photosystem II of plants. *Biochim. Biophys. Acta*, **1142** (1993) 106–14.
10. Draber, W., Kluth, J. F., Tietjen, K. & Trebst, A., Herbicides in photosynthesis research. *Angew. Chem. Int. Ed. Engl.*, **30** (1991) 1621–33.
11. Mackay, S. P. & O'Malley, P., Molecular modelling of the interactions between optically active triazine herbicides and photosystem II. *Z. Naturforsch.*, **48c** (1993) 474–81.
12. Ruffle, S. V., Donnelly, D., Blundell, T. L. & Nugent, J. H. A., A three-dimensional model of the Photosystem II reaction center of pisum sativum. *Photosyn. Res.*, **34** (1992) 287–300.
13. Bowyer, J., Hilton, M., Whitelegge, J., Jewess, P., Camillieri, P., Crofts, A. & Robinson, H., Molecular Modelling studies on the binding of phenylurea inhibitors to the D1 protein of Photosystem II. *Z. Naturforsch.*, **45c** (1990) 379–87.
14. Sobolev, V & Edelman, M., Modelling the quinone-B binding site of the photosystem II reaction center using notions of complementarity and contact-surface between atoms. *Proteins: Struct. Funct. Genet.*, **21** (1995) 214–25.
15. Ockenden, D. W. & Schofield, K., Cinnolines. XXXIII. Some 3-aryl-4-hydroxycinnolines. *J. Chem. Soc.* (1953) 3706–7.
16. Leonard, N. J. & Boyd, S. N., Cinnolines. II. Synthesis of 4-hydroxycinnolines. *J. Org. Chem.*, **11** (1946) 419–28.
17. Schofield, K. & Swain, T., Cinnolines XXI. Further observations on the Richter synthesis. *J. Chem. Soc.* (1949) 2393–9.
18. Baumgarten, H. E. & Furnas, J. L., Cinnolines. IX. The Stolle-Becher synthesis. *J. Org. Chem.*, **26** (1961) 1536–9.
19. Lowrie, H. S., 3-Phenylcinnolines. I. Some reactions and derivatives of 3-phenylcinnolines-4-carboxylic acids. *J. Med. Chem.*, **9** (1966) 664–9.
20. Bower, J. D. & Ramage, G. R., Heterocyclic systems related to pyrrocoline. II. The preparation of polyazaindenes by dehydrogenative cyclisations. *J. Chem. Soc.* (1957) 4506–10.
21. Huyser, E. S. & DeMott, D. N., *Chem. Ind.* (1963) 1954–7.
22. Bower, J. D. & Ramage, G. R., Heterocyclic systems related to pyrrocoline. I. 2 : 3a-Diazaindene. *J. Chem. Soc.* (1955) 2834–7.
23. Kröhnke, F., Krickhöfen, B. & Thoma, C., Ortsbestimmungen bei Imidazopyridinen. *Chem. Ber.*, **88** (1955) 1117–21.
24. Djerassi, C. & Pettit, G. R., Reaction of α-halo ketones with 2-pyridinthiol. *J. Am. Chem. Soc.*, **26** (1954) 4470–2.
25. Omakawa, H., Ichizen, N. & Takematsu, T. Phytotoxic studies on azine compounds. Part I. Phytotoxic properties of α-substituted benzylamino-*s*-triazines. *Agric. Biol. Chem.*, **51** (1987) 2563–8.
26. Wegner, P., Egner, U., Saenger, W. E., Gerbling, K. P., Johann, G. & Rees, R., German Patent 4·008·181, 1991.
27. Reiter, J., Pongó, L., Somorai, T. & Dvortsák, P., On triazoles. V [1,2]. Synthesis of 1- and 2-R^1-3-R^2,R^3-amino-5-amino-1,2,4-triazoles. *J. Heterocyc. Chem.*, **23** (1986) 401–8.
28. Allen, C. F. H., Beilfuss, H. R., Burness, D. M., Reynolds, G. A., Tinker, J. F. & Van Allan, J. A., The structure of certain polyazaindenes. IV. Compounds from β-keto acetals and β-methoxyvinyl ketones. *J. Org. Chem.*, **24** (1959) 796–801.
29. Brown, D. J. & Nagamatsu, T., Isomerizations akin to the Dimroth rearrangement. III. The conversion of simple *s*-triazolo[4,3-*a*]pyrimidines into their [1,5-*a*]isomers. *Austral. J. Chem.*, **30** (1977) 2515–25.
30. Latzko, E. & Gibbs, Z., Distribution and activity of enzymes of the reductive pentose phosphate cycle in spinach leaves and in chloroplasts isolated by different methods. *Pflanzenphysiol.*, **59** (1968) 184–94.
31. Goodford, P. J., A computational procedure for determining energetically favorable binding sites on biologically important macromolecules. *J. Med. Chem.*, **28** (1985), 849–57.
32. Ho, C. M. W. & Marshall, G. R., Cavity search: An algorithm for the isolation and display of cavity-like binding regions. *J. Comp.-Aided Molec. Design*, **4** (1990) 337–54.
33. Brusslan, J. & Haselkorn, R., Molecular genetics of herbicide resistance in cyanobacteria. *Photosynthesis Res.*, **17** (1988) 115–24.
34. Tietjen, K. G., Draber, W., Goossens, J., Jansen, J. R., Kluth, J. F., Schindler, M., Wroblowsky, H.-J., Hilp, U. &

Trebst, A., Binding of triazines and triazinones in the Q_B-binding niche of Photosystem II. *Z. Naturforsch.*, **48** (1993) 205–12.
35. Ebert, E. & Dumford, S. W., Effects of triazine herbicides on the physiology of plants. In *Residue Reviews 65*, ed. F. A. Gunther & J. D. Gunther. Springer-Verlag, New York Heidelberg Berlin, 1976, pp. 1–97.
36. Omakawa, H., Kobayashi, I. & Konnai, M., Phytotoxic studies on azine compounds. Part IV. Substituent effect on photosynthesis of N2-α-substituted benzyl-N4-alkyl-2, 4-diamino-6-chloro-*s*-triazines and their phytotoxic property. *Agric. Biol. Chem.*, **53** (1989) 2723–9.
37. Deisenhofer, J. & Michel, H. The photosynthetic reaction center from the purple bacterium Rhodopseudomonas viridis. *EMBO J.*, **8** (1989) 2149–70.
38. Holzenburg, A., Bewley, M. C., Wilson, F. H., Nicholson, W. V. & Ford, R. C., Three-dimensional structure of photosystem II. *Nature (London)*, **363** (1993) 470–1.
39. Fotinou, C., Kokkinidis, M., Fritsch, G., Hasase, W., Michel, H. & Ghanotakis, F., Characterization of a Photosystem II core and its three-dimensional crystals. *Photosyn. Res.*, **37** (1993) 41–8.